THE JOURNAL OF PHYSICAL CHEMISTRY A

Article

pubs.acs.org/JPCA

Dissociative Photoionization of 1-Halogenated Silacyclohexanes: Silicon Traps the Halogen

Andras Bodi,*[,†] Katrin Lilja Sigurdardottir,[‡] Ágúst Kvaran,[‡] Ragnar Bjornsson,[‡] and Ingvar Arnason[‡]

[†]Laboratory for Femtochemistry and Synchrotron Radiation, Paul Scherrer Institute, 5232 Villigen, Switzerland

[‡]Science Institute, University of Iceland, Dunhaga 3, 107 Reykjavík, Iceland

ABSTRACT: The threshold photoelectron spectra and threshold photoionization mass spectra of 1-halogenated-1-silacyclohexanes, for the halogens X = F, Cl, Br, and I, have been obtained using synchrotron vacuum ultraviolet radiation and photoelectron photoion coincidence spectroscopy. As confirmed by a similar ionization onset and density functional theory molecular orbitals, the ionization to the ground state is dominated by electron removal from the silacyclohexane ring for X = F, Cl, and Br, and from the halogen lone pair for X = I. The breakdown diagrams show that the dissociative photoionization mechanism is also different for X = I. Whereas the parent ions decay by ethylene loss for X = F to Br in the low-energy regime, the iodine atom is lost for X = I. The first step is followed by a sequential ethylene loss at higher internal energies in each of the compounds. It is argued that the tendency of silicon to lower bond angles stabilizes the complex cation in which C_2H_4 is η^2-coordinated to it, and which precedes ethylene loss. Together with the relatively strong silicon−halogen bonds and the increased inductive effect of the silacyclohexane ring in stabilizing the cation, this explains the main differences observed in the fragmentation of the halogenated silacyclohexane and halogenated cyclohexane ions. The breakdown diagrams have been modeled taking into account slow dissociations at threshold and the resulting kinetic shift. The 0 K appearance energies have been obtained to within 0.08 eV for the ethylene loss for X = F to Br (10.56, 10.51, and 10.51 eV, respectively), the iodine atom loss for X = I (10.11 eV), the sequential ethylene loss for X = F to I (12.29, 12.01, 11.94, and 11.86 eV, respectively), and the minor channels of H loss for X = F (10.56 eV) and propylene loss in X = Cl (also at 10.56 eV). The appearance energies for the major channels likely correspond to the dissociative photoionization reaction energy.

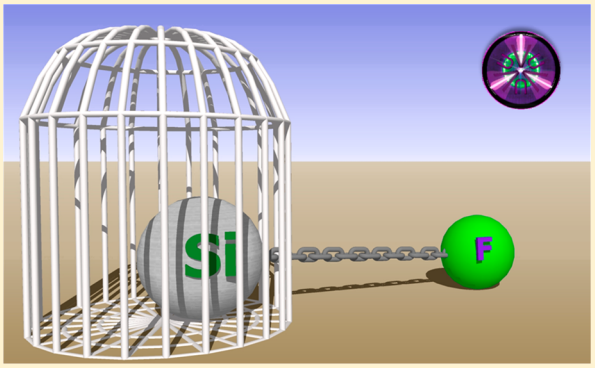

INTRODUCTION

The conformational behavior of substituted cyclohexane is one of the schoolbook examples of stereochemistry.[1] The most stable ring structure is the chair conformer. The 1,3-*syn*-diaxial repulsive interaction between bulky substituents and the axial hydrogens at C3 and C5 disfavors the axial position for the substituents and makes the equatorial position more stable; or so the story goes. The incontrovertible equatorial preference of most substituents in cyclohexane appears to be less well understood in the light of theoretical efforts, which establish the role of hyperconjugation in the conformational equilibrium,[2,3] or predict, using the theory of atoms in molecules,[4] that the *t*-butyl group is in fact more stable in the axial position, an effect counteracted by the larger destabilization of the cyclohexyl ring. In this context, it is also surprising that although some ligands, such as methyl, phenyl, and *t*-butyl, prefer the equatorial orientation in the 1-substituted silacyclohexanes,[5−9] others, e.g., halogens, or the bulkier CF_3 and SiH_3, are preferentially found in the axial position.[10−13] In addition to experimental results, this has also been confirmed consistently by *ab initio* computations,[14] and continues to be an active area of conformational studies.[15]

Despite a phenomenological correlation observed between the nuclear repulsion energies and the conformational preferences,[16] and the wealth of experimental data on a wide variety of substituents, a simple, chemically insightful, and predictive model for the conformational preference of substituted (sila)cyclohexanes has proven to be elusive. Our hope is that a deeper overall understanding of these systems will ultimately reveal an appealing rationale for the conformational behavior. Previously, the fate of silacyclohexane and 1,1-dichloro-1-silacyclohexane was studied in dissociative electron attachment (DEA).[17] No fragment formation was observed in silacyclohexane, which makes substituents suitable candidates to diagnose DEA vs dissociative ionization processes in focused electron beam induced deposition. In the chlorinated derivative, the Si−Cl bond is prone to break, and, depending on the electron energy, the negative charge is localized on either the C_5H_6Si (<1 eV) or the Cl (≈1 eV or 6−9 eV) fragments.

Received: September 11, 2016
Revised: October 31, 2016
Published: November 2, 2016

DOI: 10.1021/acs.jpca.6b09195
J. Phys. Chem. A 2016, 120, 9188−9197

With the goal to study analogous processes in the cation, we report here on the photoionization and dissociative photoionization of 1-halogenated-1-silacyclohexanes, $C_5H_{10}SiHX$ (X = F, Cl, Br, and I), studied by photoelectron photoion coincidence (PEPICO) with tunable vacuum ultraviolet (VUV) synchrotron radiation. In PEPICO, the known photon energy is expended to ionize the sample and to impart kinetic energy to the photoelectron and internal energy to the photoion.[18] When threshold, i.e., close to zero kinetic energy electrons are selected, the photoelectron signal corresponds to the threshold photoelectron spectrum (TPES), and all the excess energy above the ionization energy is available for dissociative photoionization. Thus, the internal energy of the parent ion is in fact scanned. The fractional abundance of the fragment ions can be recorded as a function of photon energy by time-of-flight mass spectrometry of the coincident photoion and plotted in the breakdown diagram. Furthermore, by imaging (i)PEPICO experiments at the VUV beamline,[19] it is also possible to measure dissociation rate constants in the 10^3−10^7 s^{-1} range, which can be modeled[20] to account for kinetic and competitive shifts and derive dissociative photoionization onsets, e.g., when the parent ion is metastable at the dissociative photoionization threshold or if quantum tunneling is at play.[21] When onsets correspond to dissociative photoionization energies, they can be used in thermochemical cycles to derive accurate thermochemical quantities.[22,23] However, since little is known about the thermochemistry of organosilicon compounds in the gas phase,[24,25] and some onsets may correspond to activation energies at tight transition states, we expect the onsets to be of limited thermochemical use. Breakdown diagrams can also give clues to complicated dissociative photoionization processes involving bond breaking and making as well as isomerization steps.[26−28] They readily identify fragmentation channels experimentally that are easily missed even in the most careful *ab initio* analysis of the potential energy surfaces,[29,30] and the quantitative characterization of the internal energy dependent unimolecular dissociation pathways can also contribute toward *ab initio* mass spectrometry.[31] We therefore expect that the silacyclohexane results will reveal the mechanisms, trends, and relative energetics of the close-lying fragmentation channels of the cations.

The comparison with cyclohexanes is of course inviting, but experimental data are scarce. Sergeev et al. have used photoionization mass spectrometry to study halogenated cyclohexanes and derive appearance energies.[32] Their results are in agreement with electron ionization mass spectra in that no halogen atom containing fragment ions were observed.[33] Thus, either the halogen atoms X or HX have to be cleaved off in the first dissociation step, and the charge remains on the carbonaceous fragments. As will be shown later, this is in contrast with the fragmentation processes of the halogenated silacyclohexanes, in which the halogen is never lost for X = F, Cl, and Br.

EXPERIMENTAL AND COMPUTATIONAL METHODS

The halogenated silacyclohexane samples were prepared as described in the literature, replicating our previous syntheses.[13,34−36] They were seeded into the ionization chamber of the iPEPICO endstation[19] at room temperature through a needle valve and a 6 mm outer diameter Teflon tube and measured at a pressure of 2−3 × 10^{-6} mbar.

Vacuum ultraviolet synchrotron radiation from the VUV beamline[37] was dispersed in grazing incidence by a 600 line/mm grating[38] and focused into a differentially pumped gas filter, in which 10 mbar of Ne or a Kr:Ar:Ne mixture was used to suppress higher harmonic radiation using an optical length of 10 cm. A 200 μm exit slit provided a photon energy resolution of 3−5 meV in the studied energy range. The light was fed into the ionization chamber, where it crossed the effusive sample beam in a constant 120 V cm^{-1} extraction field. Photoelectrons were velocity map imaged[39] onto a fast, position sensitive Roentdek delay line detector, with a better than 1 meV kinetic energy resolution at threshold. Because of their almost instantaneous detection, photoelectrons also act as start signal in the photoion time-of-flight analysis, which was carried out in first order space focus[40] using a multiple-start/multiple-stop data acquisition scheme.[41] Due to the low draw-out field, photoions spend several μs in the 5 cm long first acceleration region. If a fragmentation process takes place during this time, the time of flight of the fragment ion will be between that of the parent and the daughter, yielding a quasi-exponentially decaying daughter ion peak shape characteristic of the unimolecular dissociation rate constant.[18] These asymmetric, broadened peaks can also be characterized by their center of gravity,[42] which starts out higher and converges to the time of flight of the prompt daughter ion as the photon energy is increased and the fragmentation rate constant rises. Internal energy selection in the parent ion is achieved by selecting threshold photoionization events. Close to zero kinetic energy electrons are focused onto a small central spot on the detector. Since velocity map imaging disperses charged particles according to their momentum perpendicular to the flight axis, kinetic energy electrons with no lateral velocity component are also detected at this spot. The hot electron contamination of the center signal can be established based on a small ring area around the center spot. The corresponding mass spectrum is subtracted from the center one to obtain the threshold photoionization mass spectra as a function of photon energy.[43,44] The experimental data are reduced in three ways: (1) the threshold photoelectron yield is plotted as a function of photon energy to obtain the TPES, (2) fractional threshold ionization parent and daughter ion abundances are plotted in the breakdown diagram, and (3) daughter ion peak centers of gravity are also evaluated for slow dissociations. A statistical model is fitted to reproduce both the breakdown diagram and the center of gravity plots to obtain accurate dissociative photoionization onsets.[20]

Computational results support the interpretation of the experimental data in two ways. First, the breakdown diagram yields the stoichiometry of the fragmentation products, and its appearance hints at the dissociation mechanism, i.e., whether processes are parallel or sequential.[28] Quantum chemical calculations are used to explore the potential energy surface of the cation and locate the stationary points, namely, transition states and intermediate minima, that lead to the observed fragment ions. This is carried out with a view to find feasible pathways in the breakdown diagram energy range and to explore potential alternative channels to establish trends in compound families. Density functional theory calculations, that is, geometry optimizations, relaxed potential energy surface scans, and single point energy calculations, were carried out with the ORCA v2.9 program.[45] We used the PW6B95 hybrid functional[46] with DFT-D3(BJ) dispersion correction,[47] the def2-TZVP basis set,[48] and def2-TZVP/J auxiliary basis set

DOI: 10.1021/acs.jpca.6b09195
J. Phys. Chem. A 2016, 120, 9188−9197

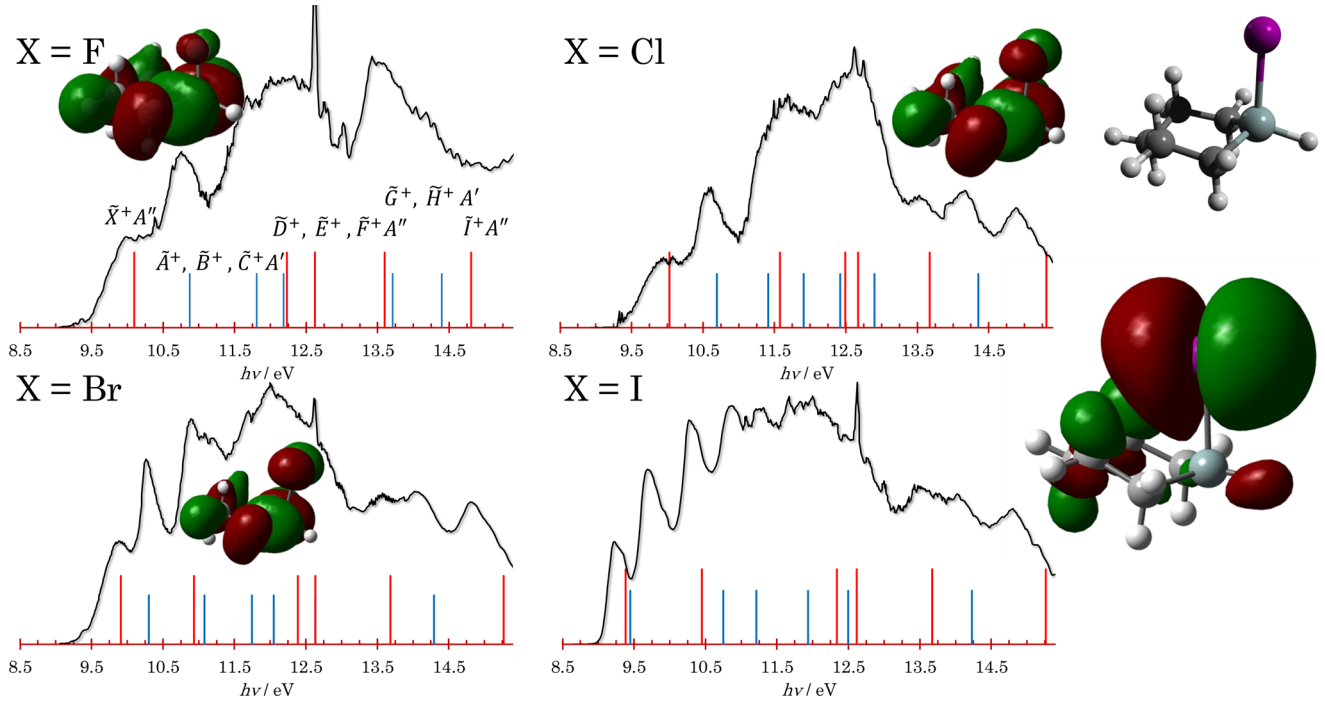

Figure 1. Threshold photoelectron spectra of 1-halogenated-1-silacyclohexanes. The sharp peaks at 12.62 eV are due to a water impurity in the chamber. The more stable, axial conformer is shown in the upper right corner, which defines the orientation of the HOMO shown for each X. Only the HOMO of X = I has a dominant halogen lone pair character. The sticks show vertical ionization energies computed using the EOM-IP-CCSD/cc-pVTZ method. The taller, red sticks denote A″ states; the shorter, blue sticks stand for A′ states. Note that the DFT HOMO for X = I is of A′ symmetry, but the EOM-IP-CCSD calculations yields an A″ ground state.

within the RIJCOSX approximation, and an effective core potential for iodine.[49−51] The Hessian was computed numerically to confirm minima and transition state geometries, and to evaluate the harmonic vibrational frequencies to obtain zero-point corrections.

The second application of the computational results is to construct the statistical model to fit the experimental breakdown diagram and measured dissociation rates. The latter can be absolute, observed in the mass spectrum (*vide supra*), or relative, in which case the relative abundances in the breakdown diagram indicate the branching ratio of two fragment ions formed in parallel and, thus, the rate constant ratio. In the statistical model,[20] the internal energy distribution of the dissociating species and the dissociation rate constants are calculated using densities and numbers of states and appearance energies, and the model threshold photoionization mass spectrum is obtained using instrument parameters, such as extraction fields and lengths. The thermal energy distribution of the sample is calculated using *ab initio* rotational constants and harmonic vibrational frequencies. Together with the photon energy and the adiabatic ionization energy, it defines the internal energy distribution of the parent ion. Dissociation rate curves are calculated within the statistical framework, which requires the density of states of the dissociating ion and the number of states of the transition state. Both are based on calculated *ab initio* harmonic vibrational frequencies and evaluated by the direct count method.[52] In the fit, the appearance energy and, for slow or competing dissociations, the transitional mode frequencies in the transition state number of states (in an RRKM model) or the rigidity factor (in an SSACM model) are fitted to reproduce the experimental data. In sequential dissociations, the excess energy is partitioned between the leaving neutral, the newly created transitional degrees of freedom, and the fragment ion using statistical theory. The latter is available for further sequential dissociation steps. Since no reverse barriers were shown to play a role in the dissociation of 1-iodo-1-silacyclohexane cations, we used the simplified statistical adiabatic channel model (SSACM), a corrected version of phase space theory, to obtain the dissociation rates,[53,54] and used the rigid activated complex Rice−Ramsperger−Kassel−Marcus (RRKM) theory for X = F to Br.[55]

Furthermore, the threshold photoelectron spectra are compared and interpreted with the help of equation of motion coupled cluster singles and doubles (EOM-IP-CCSD) calculations[56] using the cc-pVTZ basis set and an effective core potential on iodine,[57] as computed by Q-Chem.[58]

RESULTS AND DISCUSSION

Threshold Photoelectron Spectra. The TPES of $C_5H_{10}SiHX$ (X = F, Cl, Br, and I) are shown in Figure 1 for the photon energy range of 8.5 to 15 eV together with figures of the highest occupied molecular orbitals (HOMOs). Except for the iodine substituted compound, the ionization onsets lie at about 9.5 eV, and the HOMOs are localized dominantly on the silacyclohexane rings. For X = I, the ionization onset shifts down to ca. 9 eV and the HOMO corresponds dominantly to the halogen lone pair. The Kohn−Sham orbital energies can be used to predict electronically exited cationic states with respect to the ground state. The results are 0.65, 1.41, 1.85; 0.51, 1.14, 1.25; 0.25, 0.85, 1.06; and 0.03, 1.01, 1.36 eV above the ground electronic states for X = F, Cl, Br, and I, respectively.[59] The EOM-IP-CCSD results reproduce the low-energy structure in the photoelectron spectra even better except for X = I (see sticks in Figure 1). In this case, the unpaired electron is localized on the halogen, which is expected to enhance spin−

DOI: 10.1021/acs.jpca.6b09195
J. Phys. Chem. A 2016, 120, 9188−9197

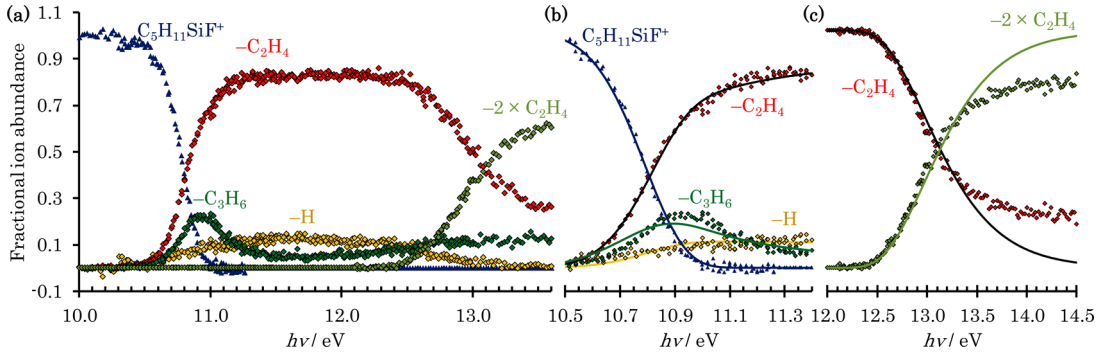

Figure 2. Overall breakdown diagram of 1-fluoro-1-silacyclohexane is shown in panel a. The RRKM model of the three low-energy channels is shown as continuous lines in panel b and of the sequential second C_2H_4 loss as continuous lines in panel c.

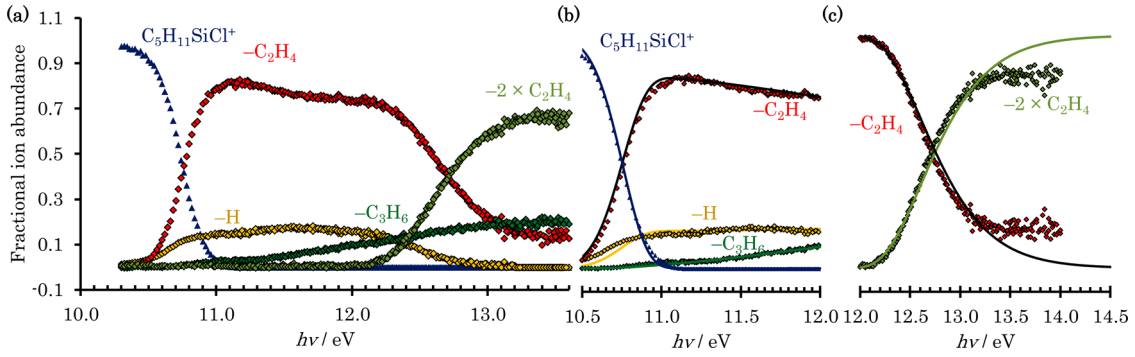

Figure 3. Overall breakdown diagram of 1-chlorosilacyclohexane is shown in panel a. The RRKM model of the three low-energy channels is shown as continuous lines in panel b and of the sequential second C_2H_4 loss as continuous lines in panel c.

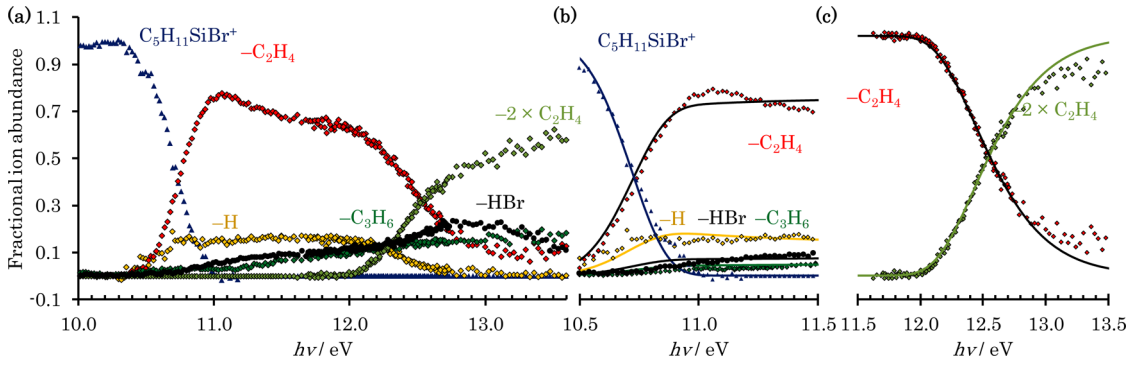

Figure 4. Overall breakdown diagram of 1-bromo-1-silacyclohexane is shown in panel a. The RRKM model of the four low-energy channels is shown as continuous lines in panel b and of the sequential second C_2H_4 loss as continuous lines in panel c.

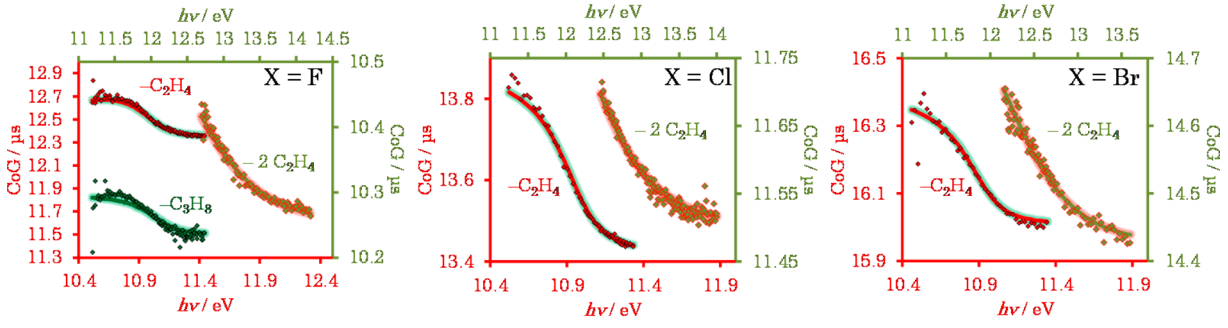

Figure 5. Daughter ion center-of-gravity fits for ethylene loss, propylene loss, and the sequential ethylene loss from fluorosilacyclohexane, for ethylene and sequential ethylene loss from chlorosilacyclohexane and bromosilacyclohexane. The low energy data are plotted along the left and bottom axes, and the top and right axes refer to sequential ethylene loss. Dots show experimental data, and continuous lines correspond to the fitted statistical model.

DOI: 10.1021/acs.jpca.6b09195
J. Phys. Chem. A 2016, 120, 9188−9197

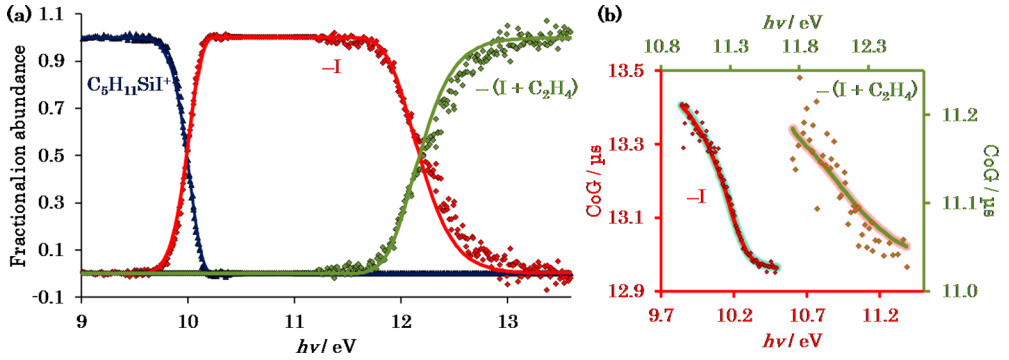

Figure 6. Experimental (dots) and modeled (continuous lines) breakdown diagram of 1-iodo-1-silacyclohexane is shown in panel a. The center of gravity of the I- and (I + C_2H_4)-loss peaks are also shown in panel b. The continuous lines are the model curves, which are based on the SSACM rate curves and are used in the extrapolation to the dissociative photoionization threshold.

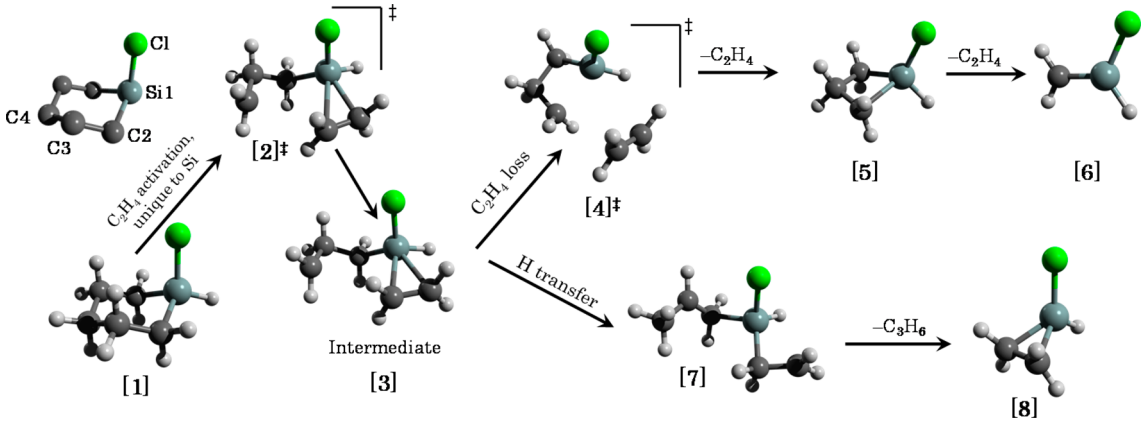

Figure 7. Dominant low-energy dissociative photoionization mechanism in 1-halogenated-1-silacyclohexanes (X = F, Cl, and Br), based on X = Cl structures with the atom numbering shown in the upper left corner. C_2H_4 activation is followed by ethylene or propylene loss, the former of which may lose a further ethylene fragment at higher energies.

orbit interaction. A spin−orbit splitting of about 0.32 eV, as to be expected in bromine containing compounds, such as CH_3Br,[60] could not be observed for X = Br because of an overlap with the next electronic state. The analogous splitting in CH_3I is about 0.62 eV,[61] which suggests that the structure in the low-energy X = I TPES is due to the combined effect of electronically excited states and spin−orbit splitting. There are photon energy ranges, in which vibrational structure is observed, such as between 10.25 and 12.5 eV for X = Cl. However, because these are hardly resolved and reliable Franck−Condon calculations are not within reach, we do not attempt to assign these progressions to normal modes. Based on the TPES, we used an adiabatic ionization energy of 9.5 eV in the modeling of the dissociative photoionization for X = F to Br and of 8.9 eV for X = I.

Breakdown Diagrams. The 1-halogenated-1-silacyclohexane breakdown diagrams are shown in Figures 2−5 and 7. It is immediately obvious that, in contrast with the halogenated cyclohexane mass spectra, the halogen atom stays in the fragment ion with the exception of X = I, in which I loss is the dominant dissociative photoionization channel at low energies. The instrumental mass resolution is comparable with the parent ion mass, which means that there is not sufficient peak shape information in the H-loss peak to obtain experimental dissociation rates. We therefore used the center of gravity of the parent ion and the H-loss bands to obtain the branching ratio between these two channels only, and the center of gravity of the C_2H_4-loss and C_3H_6-loss channels to obtain experimental rates. These are in fact characteristic of the depletion of the parent ion, hence the sum of the unimolecular dissociation rate constants, which can be apportioned to the individual channels based on the branching ratios, i.e., the relative abundances in the breakdown diagram.[42]

Based on the appearance energy range of the fragment ions and the shape of the breakdown curves, the fragmentation mechanism of the parent ion can be divided into two energy regimes. In the low energy range, below about 12 eV, parallel processes take place, such as C_2H_4 loss (the main channel for X = F, Cl, and Br), C_3H_6 and H loss (minor channels for X = F, Cl, and Br), and HX loss for X = Br. At higher energies, of about 12 eV photon energy, sequential C_2H_4 loss takes place from the main low-energy products, i.e., from the C_2H_4-loss product for X = F, Cl, and Br, and from the I-loss product for X = I. Two different mechanisms appear to be at work in the C_3H_6-loss channels. Both can be observed for X = F, where the C_2H_4- and C_3H_6-loss fragments rise in an almost parallel way, only for the C_2H_4 loss to outcompete the C_3H_6 loss at a few hundred meV higher photon energy. The C_3H_6-loss fragment ion signal then starts to rise again, albeit slowly, at 11.7 eV. The fast-rising, competitive C_3H_6-loss channels are not observed for X = Cl or Br, only the slowly rising component at somewhat lower energies than for X = F. We have only identified one reaction pathway leading to propylene loss, which involves H-transfer after a C3−C4 bond rupture in the ring (see below) and, based on the increased activation energy as F → Br, corresponds to the fast rising pathway for X = F. Although the

DOI: 10.1021/acs.jpca.6b09195
J. Phys. Chem. A 2016, 120, 9188−9197

Table 1. Appearance Energies for Neutral Fragments Derived from Statistical Modeling and Quantum Chemical Calculations (in Parentheses)

	E_0/eV				
	C_2H_4	H	C_3H_6[a]	X	$2C_2H_4/I + C_2H_4$
$C_5H_{11}SiF$	10.56 (11.03)	10.56 (10.59)	(11.01)	(13.20)	12.29 (12.76)
$C_5H_{11}SiCl$	10.51 (10.92)	(10.45)	10.56 (10.79)	(11.52)	12.01 (12.51)
$C_5H_{11}SiBr$	10.51 (10.87)	(10.46)	(10.72)	(10.93)	11.94 (12.43)
$C_5H_{11}SiI$	(10.72)	(10.32)	(10.53)	10.11 (10.26)	11.86 (12.30)

[a]The energy of the H-transfer transition state is computed to be −0.09, 0.12, 0.21, and 0.37 eV for X = F, Cl, Br, and I, respectively, relative to the dissociative photoionization reaction energy as listed.

initial transition state frequencies set for the C_3H_6-loss channels for X = Cl and Br are, therefore, unlikely to correspond to the actual transition states, the fit reproduces the branching ratios, hence the relative rates, quite well. Therefore, we still expect that the extrapolation to the threshold energy remains reasonably accurate for X = Cl.

Dissociative Photoionization Mechanism. Before proposing photoionization mechanisms, we will discuss the DFT-computed bond energies in the parent ions. The C−C, C−H, and Si−H bond energies are remarkably unchanged in the compound series, whereas the Si−X bond energy drops dramatically from X = F to I. By far the weakest C−C bond is C3−C4, which is also the weakest covalent bond in the cation and, when referenced to the neutral molecule, is broken at 10.05 (X = Cl) to 10.10 (X = I) eV, yielding η^2-bonded cations. In these species, the silicon is straddled in the π bonding molecular orbital of ethylene ([**3**] in Figure 7). Most likely, this bond breaking step leads to alkene loss observed for X = F to Br. The C−H bond energy is weakest at C3 and is broken at ca. 10.4 eV across the series. This leads to an RHC−CH_2 moiety, which is straddled by Si as in the C3−C4 bond breaking intermediate. The Si−H bond is relatively strong for X = F and weaker for X = Cl to I, with the dissociative photoionization energies decreasing from 10.5 (X = F) to 10.32 (X = I) eV. These variations are dwarfed by the decrease in the Si−X bond breaking dissociative photoionization energies (Table 1), which are calculated to drop from 13.20 (X = F) to 10.26 eV (X = I). The dominance of the I-loss process for X = I is, thereby, readily explained.

We can now propose unimolecular fragmentation mechanisms for the parent ions based on the breakdown diagrams and the computed bond energies. In the first step, the C3−C4 bonds break for X = F to Br, which yields bridged intermediates with the C_2H_4 leaving group coordinated to the Si by its η^2-bonding manner ([**1**] → [**2**]‡ → [**3**] in Figure 7). Ethylene can leave via a second transition state, [**4**]‡, in which the terminal CH_2 group moves closer to the Si and a weak C···Si bond is established. Alternatively, the Si−C bonds may also break, accompanied by H-transfer from C5 to C4, which yields propylene as the leaving neutral, and the three-membered ring $C_2H_4SiHX^+$ fragment ion ([**3**] → [**7**] → [**8**]). This propylene-loss mechanism is expected to be at play in X = F. The slow rise of the propylene-loss products at higher photon energies for X = F to Br implies another channel with a somewhat more energetic but looser transition state, meaning that the dissociation rates start rising at higher energies and do so faster. A prime candidate for such a channel would be cyclopropane formation, in which the C5···C6 bond distance decreases in the C3−C4 bond breaking intermediate. Since the C_3H_6-loss channels are generally minor, we have not explored the cyclopropane-loss channel computationally any further, and only suggest that there could be an alternative neutral fragment in the energy range of the slowly rising $C_2H_4SiHX^+$ fragments for X = F to Br.

The ethylene-loss products, $C_3H_6SiHX^+$, of a distorted four-membered-ring structure, dissociate further by a second ethylene loss to yield CH_2SiHX^+. These processes only necessitate that the C5−C6 bonds break, but they still entail a turning point along the reaction coordinate according to DFT calculations, because both the leaving neutral and the detected ionic fragments have to become planar ([**5**] → [**6**]). However, calculations indicate that the dissociation products lie marginally higher in energy than the highest lying transition state.

Besides C3−C4 bond breaking, followed by C_2H_4 or C_3H_6 loss for X = F to Br, as well as the sequential loss of a second C_2H_4 at higher energies, three further reaction channels are worth mentioning. First, H loss has been observed for X = F to Br, and, based on the bond energies, it is proposed to correspond to Si−H bond breaking, with C3−H bond breaking possibly contributing for X = F. It is worth mentioning that, according to our calculations, the C3−H is the weakest bound hydrogen atom in the unsubstituted silacyclohexane by about 50 meV, but it is stabilized by halogen substitution as opposed to the Si−H bond, which is destabilized for X = Cl, Br, and I. Second, a small amount of HX loss has been observed for X = Br, which is probably the result of H-transfer from a carbon ring atom to the halogen atom. Third, for X = I, a halogen atom loss, the sole dissociative photoionization channel below 11 eV, is followed by ethylene loss in a second, sequential step. We propose that, similar to ethylene loss from the other parent ions, this channel is also initiated by C3−C4 bond breaking, albeit in the I-loss fragment ion, after which ethylene can η^2-coordinate to the vacant Si site. The three-centered bond is broken thereafter to release C_2H_4. Reaction path calculations suggest that the transition state to the intermediate at 11.87 eV lies 0.43 eV lower than the fragments at 12.30 eV. Since these calculations do not involve iodine, they are probably quite reliable, and it is reasonable to suggest that, together with the I-loss appearance energy, the (I + C_2H_4)-loss appearance energy also corresponds to the energy of the final products and is equal to the dissociative photoionization energy.

Although the C3−C4 bond breaking transition state for C_2H_4 loss is calculated to lie lower than the energy of the final products for the X = F to Br species, the appearance energies could still be indicative of the transition state energies instead of the endothermicity of the processes, if calculations are slightly in error or if the rate-determining step is C3−C4 bond breaking at low photon energies. In sequential dissociations, we assume that the excess energy above that of the intermediate fragments is statistically distributed between the neutral and ionic fragments, and some of it is released as kinetic energy. However, energetic transition states often entail a fast

DOI: 10.1021/acs.jpca.6b09195
J. Phys. Chem. A 2016, 120, 9188−9197

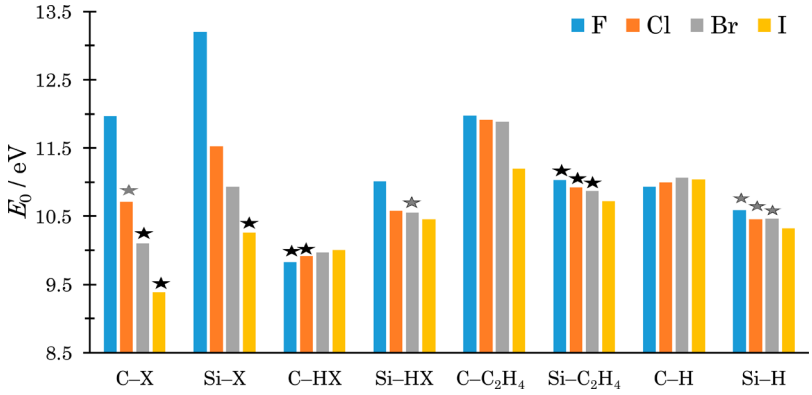

Figure 8. Comparison of the computed dissociative photoionization reaction energies in halogenated cyclohexanes (C) and silacyclohexanes (Si). Black stars mark the observed major fragmentation channels, and gray stars mark the minor channels in electron ionization mass spectra of cyclohexanes and PEPICO experiments of silacyclohexanes.

dissociation with more than the statistical amount of kinetic energy released.[62] Therefore, whereas the reported appearance energies for the sequential ethylene losses most likely correspond to the dissociative photoionization energies, strictly speaking they only constitute high limits thereto.

Statistical Model. The densities and numbers of states of the neutrals, precursors, and transition states have been calculated based on *ab initio* harmonic vibrational frequencies and rotational constants.

The daughter ion peak shapes are broadened toward higher times of flight in the onset of the energy range of both the first and the second ethylene losses for X = F to Br, and in the I and (I + C_2H_4) losses for X = I. These have also been modeled to account for the kinetic shifts. The center-of-gravity fits to account for kinetic shifts were of comparable quality for all the compounds, and are shown in Figure 6 for X = F to Br and in Figure 7b for X = I. The fact that the second ethylene-loss peaks are also broadened confirms the dissociation mechanisms and rules out concerted C_4H_8 loss, since the low-energy processes are fast on the experimental time scale at these energies, and any efficiently competing parallel processes would also have to be fast.

As seen in Figures 2–5 and 7, the main low-energy channels, i.e., the C_2H_4 losses for X = F to Br and the I loss for X = I, are reproduced well quantitatively by the fitted statistical model. In the high energy range, only the ethylene-loss intermediate ions are considered as precursors as shown in the fits in Figures 2–4c, in which the sequential ethylene losses are modeled. The fits are good at the onset of the processes, crucial for determining accurate onset energies. However, the daughter ion abundances are overestimated at higher energies, particularly for X = F, and less so for X = Br and I. This implies that, in the product energy distributions, the statistical model predicts more of the excess energy to remain as internal energy in the intermediate, single ethylene-loss ions than it actually does. The discrepancy between the fits and the experimental breakdown diagrams might, thus, hint at supra-statistical kinetic energy release, perhaps due to the impulsive nature of the first ethylene loss, once the transition state is surmounted by the system. As for the low-intensity channels, we only report appearance energies for the H loss in the case of X = F and for the C_3H_6 loss for X = Cl, which are fitted well. The C_3H_6 loss for X = F and the H loss for X = Cl are not reproduced satisfactorily to report appearance energies. A possible reason is that the flexibility in the transition state number of states during the fit is insufficient to reproduce the evolution of the branching ratios at the onset, as well as their leveling off at higher energies. Since the goodness of the fit depends much more on the latter, the onset of the breakdown curves is not modeled well. Further minor channels are too weak and the data points too scattered for X = Br to judge the quality of the model.

The derived ethylene-loss 0 K appearance energies show little variation within the series of X = F, Cl, and Br (see Table 1). Hydrogen atom loss for X = F is also seen at 10.56 eV, similar to C_3H_6 loss for X = Cl. The iodine substituted silacyclohexane, on the other hand, may only lose an iodine atom first. In the high-energy range, the breakdown diagram is dominated by a sequential ethylene loss. Because of the need to extrapolate the rate curve to the dissociation onset to account for the kinetic shift, the appearance energies listed in Table 1 are estimated to be accurate to within 0.08 eV. Since systematic errors are expected to cancel out within the compound family, the trends in the energetics, i.e., the almost constant ethylene loss appearance energy for X = F to Br, and the monotonous decrease in the appearance energy of the second ethylene loss, are expected to be accurate.

Driving Forces. Calculated appearance energies for different dissociative photoionization channels in halogenated cyclohexanes and silacyclohexanes are shown in Figure 8. As mentioned earlier, the mass spectra of the halogenated cyclohexanes are devoid of halogen-containing fragment ion peaks, whereas, among the halogenated silacyclohexanes, only the 1-iodo-1-silacyclohexane loses the halogen in the studied energy range (Scheme 1). The main reason is that silicon–halogen bonds are significantly stronger than the corresponding

Scheme 1. Comparison of the dissociative photoionization processes of halogenated cyclohexanes and silacyclohexanes

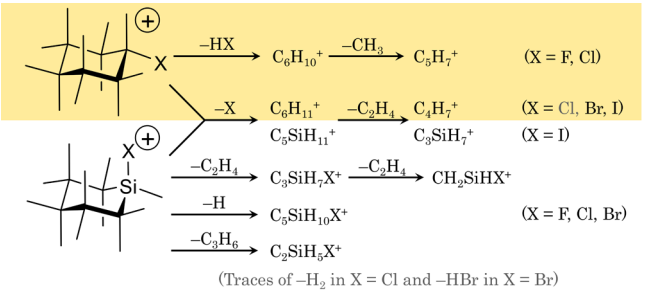

DOI: 10.1021/acs.jpca.6b09195
J. Phys. Chem. A 2016, 120, 9188–9197

carbon−halogen bonds, both in the neutral[63] and in the cation (Figure 8), which suppresses both X and HX losses in the organosilicon compounds. On the other hand, the silicon atom favors smaller bond angles, which stabilizes the C3−C4 bond breaking transition state as well as the ethylene loss products ([**2**]‡ and [**5**] in Figure 7), opening up ethylene loss as an alternative dissociative photoionization channel. While this applies to X = I, as well, the precipitous drop in the Si−I bond energy compared with Si−Br means that the ethylene-loss channel is outcompeted by halogen atom loss, and the dissociative photoionization mechanism resembles closely that of iodocyclohexane. Furthermore, because the Si−H bond is weaker than the C−H bond, hydrogen atom loss also becomes competitive for X = F−Br. We note in passing that DFT calculations underestimate the H-loss and overestimate the C_2H_4-loss thresholds. The increased halogen binding energy coupled with the more favorable ethylene-loss reaction path thus determines the dominant dissociative photoionization pathways of ethylene loss at low energies, followed by sequential ethylene loss at higher energies for X = F−Br.

CONCLUSIONS

The threshold photoelectron spectra and the dissociative photoionization of the 1-halogenated-1-silacyclohexanes for the halogen atoms X = F to I have been studied by photoelectron photoion coincidence. The ionization onsets are found to be constant at about 9 eV in the series for X = F to Br, suggesting that the ground cationic state corresponds to the removal of an electron from the silacyclohexane ring. This is confirmed by density functional theory. For X = I, on the other hand, the halogen lone pair is less bound, and the ionization takes place already at 8.5 eV. The breakdown diagrams are dominated by ethylene loss at low energies for X = F to Br, and by halogen atom loss for X = I. This is in contrast with the cyclohexane analogues, in which no halogen containing fragment ions have been observed in the electron ionization mass spectra, and X and HX losses are the lowest energy channels. At higher energies, the first dissociation for X = F−Br is followed by the sequential loss of another ethylene neutral. The propensity of the halogen atoms, F to Br, to stay in the charged fragment is explained by the stronger Si−X bonds in both the neutral and the cation, as well as the silicon atom's ability to stabilize the three-centered bond, in which a C═C moiety is η^2-coordinated to Si, making C_2H_4 loss and, to a smaller extent, C_3H_6 loss possible. The first ethylene-loss appearance energy from the parent ion is constant within the experimental uncertainty, whereas the second ethylene is lost at a decreasing energy in the X = F → Br series. Whereas calculations suggest that the first ethylene-loss fragments are at somewhat higher energies than the transition states, meaning that the appearance energies correspond to the endothermicity of the dissociative photoionizations, the apparently larger than statistical kinetic energy released in the sequential ethylene losses and the uncertainty of the calculations mean that we cannot rule out that the appearance energies correspond to reverse barriers along the dissociation coordinate. The I-loss onset for X = I, on the other hand, corresponds to the dissociative photoionization energy. However, because of the scarcity of the thermochemical anchor values for these compounds, we are yet unable to use this onset in thermochemical cycles.

The contrast between the dissociative photoionization mechanism of the halogenated cyclohexanes and the silacyclohexanes is partly due to the added conformational flexibility of the silicon atom, which has also been discussed at length in the study of the neutrals' conformational equilibria. Silicon's ability to turn ethylene into a better leaving group, combined with the higher bond energy of the Si−X bonds compared with the C−X bonds, means that the halogen substituents remain bound in the cations apart from iodosilacyclohexane.

AUTHOR INFORMATION

Corresponding Author

*E-mail: andras.boedi@psi.ch.

Notes

The authors declare no competing financial interest.

ACKNOWLEDGMENTS

Á.K. is very grateful to the Kantonsspital Baden for medical care after a biking accident suffered during the measurement campaign. The research leading to these results has received funding from the European Community's Seventh Framework Programme (FP7/2007−2013) under Grant Agreement No. 226716.

REFERENCES

(1) McMurry, J. *Organic Chemistry*; Thomson-Brooks/Cole: Belmont, 2004.

(2) Taddei, F.; Kleinpeter, E. The Anomeric Effect in Substituted Cyclohexanes. I. The Role of Hyperconjugative Interactions and Steric Effect in Monosubstituted Cyclohexanes. *J. Mol. Struct.: THEOCHEM* **2004**, *683* (1−3), 29−41.

(3) Taddei, F.; Kleinpeter, E. The Anomeric Effect in Substituted Cyclohexanes. II. The Role of Hyperconjugative Interactions and Steric Effect in 1,4-Disubstituted Cyclohexanes. *J. Mol. Struct.: THEOCHEM* **2005**, *718* (1−3), 141−151.

(4) Cortés-Guzmán, F.; Hernández-Trujillo, J.; Cuevas, G. The Nonexistence of Repulsive 1,3-Diaxial Interactions in Monosubstituted Cyclohexanes. *J. Phys. Chem. A* **2003**, *107* (44), 9253−9256.

(5) Arnason, I.; Kvaran, A.; Jonsdottir, S.; Gudnason, P. I.; Oberhammer, H. Conformations of Silicon-Containing Rings. 5. Conformational Properties of 1-Methyl-1-Silacyclohexane: Gas Electron Diffraction, Low-Temperature NMR, and Quantum Chemical Calculations. *J. Org. Chem.* **2002**, *67* (11), 3827−3831.

(6) Favero, L. B.; Velino, B.; Caminati, W.; Árnason, I.; Kvaran, Á. Structures and Energetics of Axial and Equatorial 1-Methyl-1-Silacyclohexane. *Organometallics* **2006**, *25* (16), 3813−3816.

(7) Kern, T.; Hölbling, M.; Dzambaski, A.; Flock, M.; Hassler, K.; Wallevik, S. Ó.; Arnason, I.; Bjornsson, R. Conformational Energies of Silacyclohexanes $C_5H_{10}SiHMe$, $C_5H_{10}SiH(CF_3)$ and $C_5H_{10}SiCl(SiCl_3)$ from Variable Temperature Raman Spectra. *J. Raman Spectrosc.* **2012**, *43* (9), 1337−1342.

(8) Shainyan, B. A.; Kleinpeter, E. Conformational Preferences of Si−Ph,H and Si−Ph,Me Silacyclohexanes and 1,3-Thiasilacyclohexanes. Additivity of Conformational Energies in 1,1-Disubstituted Heterocyclohexanes. *Tetrahedron* **2012**, *68* (1), 114−125.

(9) Belyakov, A. V.; Sigolaev, Y.; Shlykov, S. A.; Wallevik, S. Ó.; Jonsdottir, N. R.; Bjornsson, R.; Jonsdottir, S.; Kvaran, Á.; Kern, T.; Hassler, K.; et al. Conformational Properties of 1-Tert-Butyl-1-Silacyclohexane, $C_5H_{10}SiH(t\text{-}Bu)$: Gas-Phase Electron Diffraction, Temperature-Dependent Raman Spectroscopy, and Quantum Chemical Calculations. *Struct. Chem.* **2015**, *26* (2), 445−453.

(10) Girichev, G. V.; Giricheva, N. I.; Bodi, A.; Gudnason, P. I.; Jonsdottir, S.; Kvaran, A.; Arnason, I.; Oberhammer, H. Unexpected Conformational Properties of 1-Trifluoromethyl-1-Silacyclohexane, $C_5H_{10}SiHCF_3$: Gas Electron Diffraction, Low-Temperature NMR Spectropic Studies, and Quantum Chemical Calculations. *Chem. - Eur. J.* **2007**, *13* (6), 1776−1783.

DOI: 10.1021/acs.jpca.6b09195
J. Phys. Chem. A 2016, 120, 9188−9197

(11) Girichev, G. V.; Giricheva, N. I.; Bodi, A.; Gudnason, P. I.; Jonsdottir, S.; Kvaran, A.; Arnason, I.; Oberhammer, H. Unexpected Conformational Properties of 1-Trifluormethyl-1-Silacyclohexane, $C_5H_{10}SiHCF_3$: Gas Electron Diffraction, Low Temperature NMR, and Quantum Chemical Calculations. *Chem. - Eur. J.* **2009**, *15* (36), 8929−8929.
(12) Wallevik, S. O.; Bjornsson, R.; Kvaran, A.; Jonsdottir, S.; Arnason, I.; Belyakov, A. V.; Baskakov, A. A.; Hassler, K.; Oberhammer, H. Conformational Properties of 1-Silyl-1-Silacyclohexane, $C_5H_{10}SiHSiH_3$: Gas Electron Diffraction, Low-Temperature NMR, Temperature-Dependent Raman Spectroscopy, and Quantum Chemical Calculations. *J. Phys. Chem. A* **2010**, *114* (5), 2127−2135.
(13) Wallevik, S. Ó.; Bjornsson, R.; Kvaran, Á.; Jonsdottir, S.; Arnason, I.; Belyakov, A. V.; Kern, T.; Hassler, K. Conformational Properties of 1-Halogenated-1-Silacyclohexanes, $C_5H_{10}SiHX$ (X = Cl, Br, I): Gas Electron Diffraction, Low-Temperature NMR, Temperature-Dependent Raman Spectroscopy, and Quantum-Chemical Calculations. *Organometallics* **2013**, *32* (23), 6996−7005.
(14) Bjornsson, R.; Arnason, I. Conformational Properties of Six-Membered Heterocycles: Accurate Relative Energy Differences with DFT, the Importance of Dispersion Interactions and Silicon Substitution Effects. *Phys. Chem. Chem. Phys.* **2009**, *11* (39), 8689.
(15) Shainyan, B. A. Structure and Conformational Analysis of Silacyclohexanes and 1,3-Silaheterocyclohexanes. *Tetrahedron* **2016**, *72* (33), 5027−5035.
(16) Bodi, A.; Bjornsson, R.; Arnason, I. A Phenomenological Relationship between Molecular Geometry Change and Conformational Energy Change. *J. Mol. Struct.* **2010**, *978* (1−3), 14−19.
(17) Bjarnason, E. H.; Ómarsson, B.; Jónsdóttir, N. R.; Árnason, I.; Ingólfsson, O. Dissociative Electron Attachment and Dissociative Ionization of 1,1-Dichloro-1-Silacyclohexane and Silacyclohexane. *Int. J. Mass Spectrom.* **2014**, *370*, 39−43.
(18) Baer, T.; Sztáray, B.; Kercher, J. P.; Lago, A. F.; Bodi, A.; Skull, C.; Palathinkal, D. Threshold Photoelectron Photoion Coincidence Studies of Parallel and Sequential Dissociation Reactions. *Phys. Chem. Chem. Phys.* **2005**, *7*, 1507−1513.
(19) Bodi, A.; Johnson, M.; Gerber, T.; Gengeliczki, Z.; Sztáray, B.; Baer, T. Imaging Photoelectron Photoion Coincidence Spectroscopy with Velocity Focusing Electron Optics. *Rev. Sci. Instrum.* **2009**, *80* (3), 034101.
(20) Sztáray, B.; Bodi, A.; Baer, T. Modeling Unimolecular Reactions in Photoelectron Photoion Coincidence Experiments. *J. Mass Spectrom.* **2010**, *45* (11), 1233−1245.
(21) Bodi, A.; Baer, T.; Wells, N. K.; Fakhoury, D.; Klecyngier, D.; Kercher, J. P. Controlling Tunnelling in Methane Loss from Acetone Ions by Deuteration. *Phys. Chem. Chem. Phys.* **2015**, *17* (43), 28505−28509.
(22) Borkar, S.; Sztáray, B.; Bodi, A. Dissociative Photoionization Mechanism of Methanol Isotopologues (CH_3OH, CD_3OH, CH_3OD and CD_3OD) by iPEPICO: Energetics, Statistical and Non-Statistical Kinetics and Isotope Effects. *Phys. Chem. Chem. Phys.* **2011**, *13* (28), 13009.
(23) Bodi, A.; Csontos, J.; Kállay, M.; Borkar, S.; Sztáray, B. On the Protonation of Water. *Chem. Sci.* **2014**, *5* (8), 3057−3063.
(24) Dávalos, J. Z.; Baer, T. Thermochemistry and Dissociative Photoionization of $Si(CH_3)_4$, $BrSi(CH_3)_3$, $ISi(CH_3)_3$, and $Si_2(CH_3)_6$ Studied by Threshold Photoelectron−Photoion Coincidence S. *J. Phys. Chem. A* **2006**, *110* (27), 8572−8579.
(25) Shuman, N. S.; Spencer, A. P.; Baer, T. Experimental Thermochemistry of $SiCl_3R$ (R = Cl, H, CH_3, C_2H_5, C_2H_3, CH_2Cl, $SiCl_3$), $SiCl_3^+$, and $SiCl_3^\bullet$. *J. Phys. Chem. A* **2009**, *113* (34), 9458−9466.
(26) Hemberger, P.; Bodi, A.; Gerber, T.; Würtemberger, M. Radius, U. Unimolecular Reaction Mechanism of an Imidazolin-2-Ylidene: An iPEPICO Study on the Complex Dissociation of an Arduengo-Type Carbene. *Chem.- Eur. J.* **2013**, *19* (22), 7090−7099.
(27) Holzmeier, F.; Lang, M.; Hemberger, P.; Bodi, A.; Schäfer, M.; Dewhurst, R. D.; Braunschweig, H.; Fischer, I. Photoionization and Pyrolysis of a 1,4-Azaborinine: Retro-Hydroboration in the Cation and Identification of Novel Organoboron Ring Systems. *Chem. - Eur. J.* **2014**, *20*, 9683−9692.
(28) Heringa, M. F.; Slowik, J. G.; Prévôt, A. S. H.; Baltensperger, U.; Hemberger, P.; Bodi, A. Dissociative Ionization Mechanism and Appearance Energies in Adipic Acid Revealed by Imaging Photoelectron Photoion Coincidence, Selective Deuteration, and Calculations. *J. Phys. Chem. A* **2016**, *120* (20), 3397−3405.
(29) Yang, L.; Shroll, R. M.; Zhang, J.; Lourderaj, U.; Hase, W. L. Theoretical Investigation of Mechanisms for the Gas-Phase Unimolecular Decomposition of DMMP. *J. Phys. Chem. A* **2009**, *113* (49), 13762−13771.
(30) Liang, S.; Hemberger, P.; Neisius, N. M.; Bodi, A.; Grützmacher, H. H.; Levalois-Grützmacher, J.; Gaan, S. Elucidating the Thermal Decomposition of Dimethyl Methylphosphonate by Vacuum Ultraviolet (VUV) Photoionization: Pathways to the PO Radical, a Key Species in Flame-Retardant Mechanisms. *Chem. - Eur. J.* **2015**, *21*, 1073−1080.
(31) Bauer, C. A.; Grimme, S. How to Compute Electron Ionization Mass Spectra from First Principles. *J. Phys. Chem. A* **2016**, *120* (21), 3755−3766.
(32) Sergeev, Y. L.; Akopyan, M. E.; Vilesov, F. I.; Chizhov, Y. V. Photoionization Processes in Gaseous Cyclohexane, and Chloro- and Bromocyclohexane. *High Energy Chem.* **1973**, *7*, 369 In original 418.
(33) *NIST Chemistry WebBook, NIST Standard Reference Database Number 69*; Mallard, W. G., Linstrom, P. J., Eds.; National Institute of Standards and Technology: Gaithersburg, MD, 2013; http://webbook.nist.gov.
(34) West, R. Cyclic Organosilicon Compounds. I. Preparation of Cyclic Silanes. *J. Am. Chem. Soc.* **1954**, *76* (23), 6012−6014.
(35) Schott, G.; Schneider, P.; Kelling, H. Darstellung Und Stabilität von Aroxy-Fluor-Silanen. *Z. Anorg. Allg. Chem.* **1973**, *398* (3), 293−300.
(36) Bodi, A.; Kvaran, A.; Jonsdottir, S.; Antonsson, E.; Wallevik, S. O.; Arnason, I.; Belyakov, A. V.; Baskakov, A. A.; Holbling, M.; Oberhammer, H. Conformational Properties of 1-Fluoro-1-Silacyclohexane, $C_5H_{10}SiHF$: Gas Electron Diffraction, Low Temperature NMR, Temperature Dependent Raman Spectroscopy, and Quantum Chemical Calculations. *Organometallics* **2007**, *26* (26), 6544−6550.
(37) Johnson, M.; Bodi, A.; Schulz, L.; Gerber, T. Vacuum Ultraviolet Beamline at the Swiss Light Source for Chemical Dynamics Studies. *Nucl. Instrum. Methods Phys. Res., Sect. A* **2009**, *610* (2), 597−603.
(38) Bodi, A.; Hemberger, P.; Gerber, T.; Sztáray, B. A New Double Imaging Velocity Focusing Coincidence Experiment: i^2PEPICO. *Rev. Sci. Instrum.* **2012**, *83* (8), 083105.
(39) Eppink, A. T. J. B.; Parker, D. H. Velocity Map Imaging of Ions and Electrons Using Electrostatic Lenses: Application in Photoelectron and Photofragment Ion Imaging of Molecular Oxygen. *Rev. Sci. Instrum.* **1997**, *68* (9), 3477−3484.
(40) Wiley, W. C.; McLaren, I. H. Time of Flight Mass Spectrometer with Improved Resolution. *Rev. Sci. Instrum.* **1955**, *26*, 1150−1157.
(41) Bodi, A.; Sztáray, B.; Baer, T.; Johnson, M.; Gerber, T. Data Acquisition Schemes for Continuous Two-Particle Time-of-Flight Coincidence Experiments. *Rev. Sci. Instrum.* **2007**, *78* (8), 084102.
(42) West, B.; Joblin, C.; Blanchet, V.; Bodi, A.; Sztáray, B.; Mayer, P. M. On the Dissociation of the Naphthalene Radical Cation: New iPEPICO and Tandem Mass Spectrometry Results. *J. Phys. Chem. A* **2012**, *116* (45), 10999−11007.
(43) Sztáray, B.; Baer, T. Suppression of Hot Electrons in Threshold Photoelectron Photoion Coincidence Spectroscopy Using Velocity Focusing Optics. *Rev. Sci. Instrum.* **2003**, *74* (8), 3763−3768.
(44) Bodi, A.; Hemberger, P. Imaging Breakdown Diagrams for Bromobutyne Isomers with Photoelectron-Photoion Coincidence. *Phys. Chem. Chem. Phys.* **2014**, *16* (2), 505−515.
(45) Neese, F. The ORCA Program System. *Wiley Interdiscip. Rev. Comput. Mol. Sci.* **2012**, *2* (1), 73−78.
(46) Zhao, Y.; Truhlar, D. G. Design of Density Functionals That Are Broadly Accurate for Thermochemistry, Thermochemical Kinetics, and Nonbonded Interactions. *J. Phys. Chem. A* **2005**, *109* (25), 5656−5667.

DOI: 10.1021/acs.jpca.6b09195
J. Phys. Chem. A 2016, 120, 9188−9197

(47) Grimme, S.; Antony, J.; Ehrlich, S.; Krieg, H. A Consistent and Accurate Ab Initio Parametrization of Density Functional Dispersion Correction (DFT-D) for the 94 Elements H-Pu. *J. Chem. Phys.* **2010**, *132* (15), 154104.
(48) Weigend, F.; Ahlrichs, R. Balanced Basis Sets of Split Valence, Triple Zeta Valence and Quadruple Zeta Valence Quality for H to Rn: Design and Assessment of Accuracy. *Phys. Chem. Chem. Phys.* **2005**, *7* (18), 3297−3305.
(49) Weigend, F. Accurate Coulomb-Fitting Basis Sets for H to Rn. *Phys. Chem. Chem. Phys.* **2006**, *8* (9), 1057.
(50) Neese, F.; Wennmohs, F.; Hansen, A.; Becker, U. Efficient, Approximate and Parallel Hartree−Fock and Hybrid DFT Calculations. A "Chain-of-Spheres" Algorithm for the Hartree−Fock Exchange. *Chem. Phys.* **2009**, *356* (1−3), 98−109.
(51) Peterson, K. A.; Figgen, D.; Goll, E.; Stoll, H.; Dolg, M. Systematically Convergent Basis Sets with Relativistic Pseudopotentials. II. Small-Core Pseudopotentials and Correlation Consistent Basis Sets for the Post-D Group 16−18 Elements. *J. Chem. Phys.* **2003**, *119* (21), 11113.
(52) Beyer, T.; Swinehart, D. R. Number of Multiply-Restricted Partitions. *Commun. ACM* **1973**, *16*, 379.
(53) Stevens, W.; Sztáray, B.; Shuman, N. S.; Baer, T.; Troe, J. Specific Rate Constants k(E) of the Dissociation of the Halobenzene Ions: Analysis by Statistical Unimolecular Rate Theories. *J. Phys. Chem. A* **2009**, *113* (3), 573−582.
(54) Bodi, A.; Kvaran, Á.; Sztáray, B. Thermochemistry of Halomethanes CF_nBr_{4-n} (n = 0−3) Based on iPEPICO Experiments and Quantum Chemical Computations. *J. Phys. Chem. A* **2011**, *115* (46), 13443−13451.
(55) Baer, T.; Hase, W. L. *Unimolecular Reaction Dynamics: Theory and Experiments*; Oxford University Press: New York, 1996.
(56) Stanton, J. F.; Bartlett, R. J. The Equation of Motion Coupled-Cluster Method. A Systematic Biorthogonal Approach to Molecular Excitation Energies, Transition Probabilities, and Excited State Properties. *J. Chem. Phys.* **1993**, *98* (9), 7029.
(57) Peterson, K. A.; Shepler, B. C.; Figgen, D.; Stoll, H. On the Spectroscopic and Thermochemical Properties of ClO, BrO, IO, and Their Anions. *J. Phys. Chem. A* **2006**, *110* (51), 13877−13883.
(58) Shao, Y.; Molnar, L. F.; Jung, Y.; Kussmann, J.; Ochsenfeld, C.; Brown, S. T.; Gilbert, A. T. B.; Slipchenko, L. V.; Levchenko, S. V.; O'Neill, D. P.; et al. Advances in Methods and Algorithms in a Modern Quantum Chemistry Program Package. *Phys. Chem. Chem. Phys.* **2006**, *8* (27), 3172−3191.
(59) Gengeliczki, Z.; Pongor, C. I.; Sztáray, B. Assigning Photoelectron Spectra of Transition Metal Organometallic Complexes on the Basis of Kohn−Sham Orbital Energies. *Organometallics* **2006**, *25* (10), 2553−2560.
(60) Urban, B.; Bondybey, V. E. One-Color Multiphoton Threshold Photoelectron Spectra of Methyl Bromide, and Their Comparison with Methyl Iodide. *J. Chem. Phys.* **2002**, *116* (12), 4938.
(61) Kimura, K.; Katsumata, S.; Achiba, Y.; Matsumoto, H.; Nagakura, S. Photoelectron Spectra and Orbital Structures of Higher Alkyl Chlorides, Bromides, and Iodides. *Bull. Chem. Soc. Jpn.* **1973**, *46* (2), 373−380.
(62) Harvey, J.; Bodi, A.; Tuckett, R. P.; Sztáray, B. Dissociation Dynamics of Fluorinated Ethene Cations: From Time Bombs on a Molecular Level to Double-Regime Dissociators. *Phys. Chem. Chem. Phys.* **2012**, *14* (11), 3935.
(63) Bodie, E. D.; McDaniel, D. H.; Alexander, J. J. *Concepts and Models of Inorganic Chemistry*, 3rd ed.; John Wiley and Sons, Inc.: 1994.

DOI: 10.1021/acs.jpca.6b09195
J. Phys. Chem. A 2016, 120, 9188−9197